Quadrupolar photovoltaic effect in the terahertz range in a two-dimensional spin-$\frac{3}{2}$ hole system

Mohsen Farokhnezhad,[1] W. A. Coish,[2] Reza Asgari,[3,4] and Dimitrie Culcer[3,5]
[1]*School of Nano Science, Institute for Research in Fundamental Sciences (IPM), Tehran 19395-5531, Iran*
[2]*Department of Physics, McGill University, 3600 rue University, Montreal, Qc H3A 2T8, Canada*
[3]*School of Physics, The University of New South Wales, Sydney 2052, Australia*
[4]*School of Physics, Institute for Research in Fundamental Sciences (IPM), Tehran 19395-5531, Iran*
[5]*Australian Research Council Centre of Excellence in Future Low-Energy Electronics Technologies, UNSW Sydney, Sydney 2052, Australia*

(Received 2 May 2022; revised 3 January 2023; accepted 26 January 2023; published 8 February 2023)

The quantum kinetic approach based on the density matrix offers a complete quantum mechanical description of dynamical optical and transport currents in solid-state systems. Starting from the quantum Liouville equation for the density matrix in an external electric field, we identify a strong photovoltaic response due to the nonlinear optical transition between heavy and light hole sub-bands enabled by T_d symmetry in a quantum well, which we term the *quadrupolar photovoltaic effect* (QPE). The photovoltaic current exhibits a strong resonance in the vicinity of the heavy hole-light hole splitting, with a magnitude governed by the momentum relaxation time, which can reach nanoseconds in GaAs holes. Since the heavy hole-light hole splitting can be tuned from a few meV to nearly 100 meV, the QPE could serve as the basis for a terahertz photodetector, addressing the famous *terahertz gap*. We discuss experimental observation and device applications.

DOI: 10.1103/PhysRevB.107.085405

I. INTRODUCTION

The past decade has witnessed a spectacular resurgence in the study of nonlinear electromagnetic effects, motivated by the rise of topological materials and cutting-edge developments in semiconductors [1–12]. Second-order responses require inversion symmetry breaking and this is satisfied by most topological materials, which has led to discoveries such as Hall effects [13–15] in time-reversal invariant systems and advances in generating nonreciprocal currents [16–19]. Among the latter, photocurrents are intimately related to the Hilbert space topology and underlie photovoltaic devices [5,20–37], with potential applications in solar cells, energy harvesting, and terahertz devices [38–43].

Recent years have witnessed a flurry of interest in holes in III-V zinc-blende semiconductors such as GaAs, which have a spin-$\frac{3}{2}$, enabling physics that is impossible in spin-$\frac{1}{2}$ electron systems. Hole systems have been synthesised to high quality, exhibiting very large mobilities, display strong topological effects [44–54], and are intensively studied for all-electrical quantum computing applications [55–58]. Until recently, inversion-breaking tetrahedral-symmetry terms were believed to be negligible for holes [59]. Hence, photovoltaic effects, which require inversion symmetry breaking, have not been investigated in purely hole systems. Yet, recent research [60] has revealed that tetrahedral-symmetry terms can be large, and the combination of spin-$\frac{3}{2}$ and tetrahedral symmetry results in a quadrupole spin-orbit interaction with electric fields. This interaction opens the door to photovoltaic applications in the elusive terahertz range. We note that similar terms may be present in low-dimensional diamond structures in Si and Ge, but they stem from the interface and their magnitude must be determined for individual geometries [61].

In this paper, we determine the full photovoltaic response of a doped asymmetric hole GaAs quantum well and identify a strong resonance due to optical transitions between the lowest light hole (LH) and heavy hole (HH) subbands. We refer to this as the *quadrupolar photovoltaic effect* (QPE), since, in the spherical tensor decomposition of the spin density matrix, the HH-LH splitting can be understood as a (spin) quadrupole moment of hole systems with an effective spin $j = \frac{3}{2}$ [62]. The optical transition is caused by tetrahedral symmetry terms that go beyond the Luttinger Hamiltonian and are responsible for an asymmetry in transition rates across the Fermi surface. The effect relies on finite doping and disorder and is not captured by a naive application of Fermi's golden rule. Whereas photovoltaic effects have a long history in noncentrosymmetric semiconductors [63,64], all the examples studied in the past involved transitions between the valence and conduction bands rather than between valence subbands, as we find here. More importantly, the QPE enables high-quality photodetectors in the elusive terahertz regime, addressing the famous *terahertz gap* [39,40,65–67]. This endows the QPE with significant practical utility: THz radiation passes through industrial materials, enabling inspection of packaged products and quality checks. Thanks to its low energies, it does not damage tissues or cause cancer, making it suitable for security detectors. Conventional photodetecting techniques do not work in the THz regime because there are no real materials with energy gaps in the range 1–100 meV

[39,40,65–67]. Only strained twisted bilayer graphene has recently been reported to be useful in the THz regime, according to calculations in Ref. [68]. Hence, the QPE addresses a fundamental gap: the energies involved lie in the THz range and the HH-LH splitting can be adjusted by the top gate field over the entire THz range, as we show below.

The paper is organized as follows. In Sec. II, an effective model Hamiltonian for a 2D hole GaAs system and theoretical quantum kinetic theory to calculate the second-order optical current are provided. We discuss an electric-dipole term which emerges in an asymmetric quantum well and provide a 2×2 effective Hamiltonian to describe the $m_z=\frac{3}{2}$ and $m_z=-\frac{1}{2}$ states. Then, we calculate both diagonal and off-diagonal components of the density matrix and, afterward, the nonlinear optical current is obtained. In Sec. III, we provide our numerical results showing the optical transitions between the LH and HH bands. In addition, the impact of the contribution of the Dresselhaus spin-orbit interaction on the QPE is investigated. Finally, we summarize our main results in Sec. IV.

II. MODEL AND THEORY

A. Effective Hamiltonian for a 2D hole GaAs system

We study a hole quantum well (QW) in GaAs where the first HH subband is occupied while the first LH subband is unoccupied. We consider an effective low-energy model Hamiltonian at zero temperature for the system, and then we utilize the density matrix method to calculate the nonlinear optical current.

The hole dispersion relation in quantum well structures is determined by the strong spin-orbit interaction in the Luttinger Hamiltonian [59]. The 4×4 Luttinger Hamiltonian, $\mathcal{H}_L$, describes the valence band of common diamond and zinc-blende semiconductors. In the spherical approximation, it takes the form $\mathcal{H}_L=\frac{\hbar^2}{2m}[(\gamma_1+\frac{5}{2}\gamma_2)k^2I_4-2\gamma_2(\boldsymbol{k}\cdot\mathbf{J})^2]$, where $\boldsymbol{J}$ represents the vector of spin-$\frac{3}{2}$ matrices, analogous to the customary vector of Pauli matrices in electron systems. For GaAs, the Luttinger parameters are $\gamma_1=6.85$ and $\gamma_2=2.10$. We consider an asymmetric QW formed at a heterointerface along the z direction, where the Cartesian coordinates are aligned with the main crystal symmetry axis. In a QW, size quantization leads to a spin quantization axis along the confinement direction, so the HH states have $m_z=\pm\frac{3}{2}$ and the LH states have $m_z=\pm\frac{1}{2}$. The asymmetric confinement can be described by a triangular potential $V(z)=-eF_zz$ for $z>0$ and ∞ otherwise, where $e=-|e|$ is the electron charge and $\mathbf{F}=F_z\hat{z}$ is the interface electric field. The band Hamiltonian $\mathcal{H}_0$ for the QW, including the confinement potential, is written as $\mathcal{H}_0=\mathcal{H}_L+V(z)I_4+\mathcal{H}_{d_z}$, where I_4 is the 4×4 identity matrix. The band Hamiltonian includes an electric-dipole term, $\mathcal{H}_{d_z}$, which emerges as a result of T_d symmetry [59] in an asymmetric QW, where the inversion asymmetry is induced by a static top gate electric field. This term has been omitted in previous studies due to the belief that its size is negligible, yet Ref. [60] demonstrated that it is large in zinc-blende materials such as GaAs. The explicit form of the electric-dipole term $\mathcal{H}_{d_z}$ induced by a triangular potential (due, e.g., to a top gate) is [60] $\mathcal{H}_{d_z}=\frac{1}{\sqrt{3}}ea_B\chi F_z\{J_x,J_y\}$, with $ea_B\simeq 2.5\text{D}$ (a_B is the Bohr radius and D is a Debye), while χ is a parameter that controls the strength of the electric-dipole matrix elements. This term couples the $m_z=\frac{3}{2}$ and $m_z=-\frac{1}{2}$ states, as well as $m_z=-\frac{3}{2}$ to $m_z=\frac{1}{2}$, allowing for HH-LH transitions that would otherwise be forbidden. In the language of spherical tensors, this term constitutes a spin quadrupole [59].

The band Hamiltonian $\mathcal{H}_0$ can be simplified using second-order perturbation theory [60]. This reduces it to two copies of the following 2×2 effective Hamiltonian:

$$\mathcal{H}_{\text{eff}}=\varepsilon_0\mathbb{1}-\frac{\Delta\epsilon}{2}\sigma_z+(\lambda' k+\gamma_1' k^3+\gamma_2' k^5+\gamma_{R3}k^7)\times(ie^{-i\theta}\sigma_+ +\text{H.c.}),\tag{1}$$

where $\boldsymbol{k}=k_x\hat{\boldsymbol{x}}+k_y\hat{\boldsymbol{y}}$, $\varepsilon_0=(\epsilon_1+\epsilon_2)/2$, $\epsilon_{1(2)}=\epsilon^1_{\text{HH(LH)}}+(\gamma_1+\gamma_2)\frac{\hbar^2k^2}{2m}$, $k_\pm=k_x\pm ik_y$, $\sigma_\pm=(\sigma_x\pm i\sigma_y)/2$, $\Delta\epsilon=\epsilon_2-\epsilon_1$, the third term represents the Rashba spin-orbit coefficients as $\lambda'=\lambda+\beta_{\chi 1}\sin 2\theta$, $\lambda=\frac{\sqrt{3}\hbar^2}{m}\gamma_2\int_0^\infty dz F^1_{\text{HH}}(z)\frac{d}{dz}F^1_{\text{LH}}(z)$, where $F^n_{\text{i}}(z)$ are the envelopes given by Airy functions, $\gamma_1'=\gamma_{R1}+\beta_{\chi 2}\sin 2\theta$, $\gamma_2'=\gamma_{R2}+\beta_{\chi 3}\sin 2\theta$, where $\theta=\arctan(k_y/k_x)$ is the polar angle of the wave vector $\mathbf{k}$. Note that only odd powers of k are permitted since inversion symmetry is broken, while time-reversal symmetry is preserved. For the range of the considered electric fields, we find that the linear Rashba spin-orbit coupling has a similar order to the cubic Rashba spin-orbit coupling. The coefficients of the Rashba spin-orbit coupling $\gamma_{R(n=1,2,3)}$ can be calculated as

$$\gamma_{Rn}=\frac{(-1)^n}{(2n-1)!}\ell^{2n}\left(\frac{2}{\lambda}\right)^{2n-1},\tag{2}$$

where $\ell=-\sqrt{3}\hbar^2\xi\gamma_2/2m$. In addition, the dipolar spin-orbit coupling terms $\beta_{\chi n=1,2,3}$, which arise from finite electric-dipole matrix elements ($\mathcal{H}_d$ with $\chi\neq 0$), can be written as

$$\beta_{\chi n}=\frac{2n}{\ell}\gamma_{Rn}ea_B\chi F_z\xi,\tag{3}$$

where $\xi=\int_0^\infty dz F^1_{\text{HH}}(z)F^1_{\text{LH}}(z)$. We stress that $\mathcal{H}_{\text{eff}}$ is written in the basis $\{\frac{3}{2},-\frac{1}{2}\}$, in which one state represents HHs and the other LHs, using the methodology of Ref. [69]. An additional copy of this matrix exists for $\{-\frac{3}{2},\frac{1}{2}\}$. Our notation is somewhat unconventional, which leads to the unusual form for the Rashba terms. The term $\propto\beta_{\chi 2}$ is of the same order as the Rashba spin-orbit coefficients, demonstrating its indispensability for a quantitative theory of hole dynamics in asymmetric GaAs QWs. This term vanishes when $\chi=0$, showing that the dipolar spin-orbit coupling is, therefore, necessary for a quantitative theory of the spin-orbit couplings for HHs in asymmetric GaAs QWs.

The dispersion relations of the effective Hamiltonian are obtained as

$$\varepsilon_k^s=\varepsilon_0+s\sqrt{\left(\frac{\Delta\epsilon}{2}\right)^2+(\lambda' k+\gamma_1' k^3+\gamma_2' k^5+\gamma_{R3}k^7)^2},\tag{4}$$

where $s=\pm$ and, furthermore, the eigenvectors of the system are given by

$$u^s_{\mathbf{k}}=\frac{1}{\sqrt{2h(k,\theta)}}\begin{pmatrix}s\sqrt{h(k,\theta)-s\frac{\Delta\epsilon}{2}}\\ -i\sqrt{h(k,\theta)+s\frac{\Delta\epsilon}{2}}e^{i\theta}\end{pmatrix},\tag{5}$$

where $h(k,\theta)$ equals

$$h(k,\theta)=\sqrt{\left(\frac{\Delta\epsilon}{2}\right)^2+(\lambda' k+\gamma_1' k^3+\gamma_2' k^5+\gamma_{R3}k^7)^2}. \quad (6)$$

B. Kinetic theory and density matrix approach

Since the photovoltaic effect is a kinetic phenomenon [70], we formulate a full quantum kinetic theory based on the density matrix [71–73], which captures interband transitions induced by electric fields as well as disorder. We work in the crystal momentum representation $|\mathbf{k},s\rangle=e^{i\mathbf{k}\cdot\mathbf{r}}|u^s_{\mathbf{k}}\rangle$, where $|u^s_{\mathbf{k}}\rangle$ is the lattice-periodic part of the Bloch wave function. We commence with the quantum Liouville equation for the time-dependent single particle density matrix $f_{\boldsymbol{k}}(t)$ averaged over the disorder configuration in momentum space [73],

$$\frac{\partial f_{\boldsymbol{k}}(t)}{\partial t}+\frac{i}{\hbar}[\mathcal{H}_{\boldsymbol{k}},f_{\boldsymbol{k}}(t)]=0, \quad (7)$$

where $\mathcal{H}_{\boldsymbol{k}}$ is the total Hamiltonian of the system including the light-matter interaction,

$$\mathcal{H}=\mathcal{H}_{\rm eff}+U(\mathbf{r})+\mathcal{H}_E+\mathcal{H}_{d_x}, \quad (8)$$

where $U(\mathbf{r})$ is the impurity potential and the time-dependent external field of a monochromatic light wave, $\mathcal{H}_E=-e\mathbf{E}\cdot\hat{\mathbf{r}}$ represents the perturbed interaction with the external electric field in the length gauge, and $\hat{\mathbf{r}}$ is the position operator. For concreteness, we henceforth consider $\boldsymbol{E}\parallel\hat{\boldsymbol{x}}$, where $\hat{\boldsymbol{x}}$ is aligned with the [100] crystal axis, $\mathcal{H}_E=-eE_x\cos(\omega t)\hat{x}$. The electric-dipole term along $\hat{x}$, which is the main term responsible for the QPE, is given by

$$\mathcal{H}_{d_x}=\frac{1}{\sqrt{3}}ea_B\chi E_x\{J_y,J_z\}. \quad (9)$$

Notice again J_y and J_z are the components of the vector of spin-$\frac{3}{2}$ matrices.

Having written the total Hamiltonian, which breaks parity and preserves time reversal, the quantum kinetic equation describing the dynamics of the impurity-averaged density matrix $f_{\boldsymbol{k}}$ takes the form

$$\frac{\partial f_{\boldsymbol{k}}(t)}{\partial t}+\frac{i}{\hbar}[\mathcal{H}_{{\rm eff},\mathbf{k}},f_{\boldsymbol{k}}(t)]+J(f_{\boldsymbol{k}}(t))=-\frac{i}{\hbar}[\mathcal{H}_E+\mathcal{H}_{d_x},f_{\boldsymbol{k}}(t)], \quad (10)$$

where $J[f_{\boldsymbol{k}}(t)]$ is the scattering term due to impurities. We approximate the scattering term [73] as $J[f_{\boldsymbol{k}}(t)]=f_{\boldsymbol{k}}(t)/\tau(\boldsymbol{k})$, where $\tau(\boldsymbol{k})$ is a time taken to relax the hot charge carriers toward the equilibrium state. To calculate the $\tau(\boldsymbol{k})$ by making use of Fermi's golden rule, we consider $U(r,\theta)=U_0\sum_i\delta(\mathbf{r}-\mathbf{r}_i)+U_0\sum_i(\mathbf{r}-\mathbf{r}_i)\cos\theta$ as a sum of short-range and asymmetric scattering potentials, respectively. After lengthy but straightforward calculations [74], the time $\tau(\mathbf{k})$ is given by

$$\begin{aligned}\frac{1}{\tau(k,\theta)}=\frac{1}{\tau_0}\Bigg[1+\frac{1}{2\pi}\int d\theta'\Bigg(&-\frac{3B\partial_k h(k,\theta')}{2A^2k^3}+\frac{3B^2}{4A^2k^4}+\frac{1}{2}\left(\frac{\partial_k h(k,\theta')}{Ak}\right)^2+\frac{B\partial_k^2 h(k,\theta')}{2A^2k^2}\Bigg)\Bigg]\\&+\frac{1}{\tau_0(k)}\Bigg(1-\frac{3}{2A^2k^3}\Bigg[f_1\partial_k f_1+\frac{1}{2}f_2\partial_k f_2-h(k,\theta)\sqrt{\left(\frac{\Delta\varepsilon}{2}\right)^2+f_1^2}\left(\frac{\partial_k f_1}{f_1}-\frac{\partial_k f_2}{f_2}\left(\frac{\Delta\varepsilon}{2f_1}\right)^2\right)\Bigg]\\&+\frac{1}{2(Ak)^2}\Bigg[(\partial_k f_1)^2+f_1\partial_k^2 f_1+\frac{1}{2}\left(f_2\partial_k^2 f_2+(\partial_k f_2)^2\right)-h(k,\theta)\sqrt{\left(\frac{\Delta\varepsilon}{2}\right)^2+f_1^2}\left(\frac{\partial_k^2 f_1}{f_1}+\frac{\partial_k^2 f_2}{f_2}+2\frac{\partial_k f_1}{f_1}\frac{\partial_k f_2}{f_2}\right.\\&\left.+\frac{1}{9}\left(\left(\frac{\partial_k f_1}{f_1}+\frac{\partial_k f_2}{f_2}\right)^2+2\frac{\partial_k f_2}{f_2}\frac{\partial_k f_1}{f_1}\right)-\frac{((\partial_k f_2)^2+f_2\partial_k f_2)\left[\left(\frac{\Delta\varepsilon}{2}\right)^2+f_1^2\right]}{(f_1 f_2)^2}-\frac{2}{3}\frac{(\partial_k f_1)^2}{\left[\left(\frac{\Delta\varepsilon}{2}\right)^2+f_1^2\right]}\left(1+\frac{f_1\partial_k f_2}{f_2\partial_k f_1}\right)\right)\Bigg]\Bigg),\end{aligned} \quad (11)$$

where $A=\hbar^2(\gamma_1+\gamma_2)/2m$, $B=h(k,\theta')-h(k,\theta)$, $f_1=\lambda k+\gamma_{R1}k^3+\gamma_{R2}k^5+\gamma_{R3}k^7$, $f_2=\beta_{\chi 1}k+\beta_{\chi 2}k^3+\beta_{\chi 3}k^5$, $\tau_0=\hbar^3(\gamma_1+\gamma_2)/(n_i m U_0^2)$, and $\tau_0(k)=A\hbar k^6/2\pi^2 n_i U_0^2$ with n_i is the impurity density. For numerical purposes, we average over θ and $k=k_F$ to approximate $\tau(k,\theta)$ with a constant τ.

To evaluate the QPE, the impurity-averaged density matrix, $f_{\boldsymbol{k}}$, is expanded systematically in powers of the electric field as $f_{\boldsymbol{k}}(t)=f_{\boldsymbol{k}}^{(0)}+f_{\boldsymbol{k}}^{(1)}(t)+f_{\boldsymbol{k}}^{(2)}(t)+\ldots$ [73], where $f_{\boldsymbol{k}}^{(0)}$ is the equilibrium density matrix, which is diagonal, with matrix elements equal to the Fermi-Dirac distribution for each band. We assume the temperature to be absolute zero. The density matrix for a two-band model can be decomposed into the diagonal, $f_{\boldsymbol{k},d}(t)$ and off-diagonal, $f_{\boldsymbol{k},od}(t)$ parts in the band basis representation. Therefore, Eq. (10) becomes

$$\begin{aligned}\frac{\partial f_d^n}{\partial t}+\frac{i}{\hbar}\left[\mathcal{H}_{\rm eff},f_d^n\right]+\frac{f_d^n}{\tau}&=-\frac{i}{\hbar}\left[\mathcal{H}_E+\mathcal{H}_{d_x},f_d^{(n-1)}\right],\\\frac{\partial f_{od}^n}{\partial t}+\frac{i}{\hbar}\left[\mathcal{H}_{\rm eff},f_{od}^n\right]+\frac{f_{od}^n}{\tau}&=-\frac{i}{\hbar}\left[\mathcal{H}_E+\mathcal{H}_{d_x},f_{od}^{(n-1)}\right],\end{aligned} \quad (12)$$

where we ignore the cross contributions of the scattering terms; $J_d(f_{od}^n)=J_{od}(f_d^n)=0$. The conventional driving term, stemming from the commutator $-(i/\hbar)[\mathcal{H}_E,f_{\boldsymbol{k}}(t)]$, takes the form $(e\boldsymbol{E}/\hbar)\cdot(\nabla_{\mathbf{k}}f_{\boldsymbol{k}}(t)-i[\boldsymbol{\mathcal{R}}_{\boldsymbol{k}},f_{\boldsymbol{k}}(t)])$. The Berry connection $\boldsymbol{\mathcal{R}}_{\boldsymbol{k}}^{ss'}=\langle u_{\boldsymbol{k}}^s|i\nabla_{\boldsymbol{k}}|u_{\boldsymbol{k}}^{s'}\rangle$ is a vector in real space as well as a matrix in the Hilbert space spanned by the lattice-periodic

Bloch wave. Notice that the condition $\mathcal{R}_{\boldsymbol{k}}^{ss'} = \mathcal{R}_{\boldsymbol{k}}^{*,s's}$ is satisfied. The conventional driving term by itself does not yield a second-order electrical response in a spin-$\frac{3}{2}$ hole system, but the dipolar term $\mathcal{H}_{d_x}$ does. Therefore, we have a new term in the covariant derivative:

$$-\frac{i}{\hbar}\langle[\mathcal{H}_E + \mathcal{H}_{d_x}, f^{(n-1)}]\rangle = \frac{e\mathbf{E}}{\hbar}\cdot\left[\nabla_{\mathbf{k}} f^{(n-1)} - i\Gamma_{\mathbf{k}}^{ss'}\left(f^{(n-1)}(\varepsilon_{\mathbf{k}}^{s}) - f^{(n-1)}(\varepsilon_{\mathbf{k}}^{s'})\right)\right], \tag{13}$$

where $\Gamma_{\mathbf{k}}^{ss'} = \mathcal{R}_{\mathbf{k}}^{ss'} - a_B\chi\xi\Lambda_{\mathbf{k}}^{ss'}$, $\Lambda_{\mathbf{k}}^{ss'} = (\zeta_k + (1-\alpha k^2)\Omega_k)\hat{x}$ with $\alpha = (\ell/\lambda)^2$ [more details about the matrix $\Lambda_{\mathbf{k}}^{ss'}$ are presented in Supplemental Material (SM) Sec. III].

The lengthy expansion procedure is performed in the Supplemental Material and can be summarized as follows. First, in linear response, one calculates $f_{\boldsymbol{k}}^{(1)}$, hence in the driving term on the right-hand side (RHS) of Eq. (10), one replaces $f_{\boldsymbol{k}} \to f_{\boldsymbol{k}}^{(0)}$. Next, to determine $f_{\boldsymbol{k}}^{(2)}$, the procedure is repeated, except now on the RHS of Eq. (10) we have $f_{\boldsymbol{k}} \to f_{\boldsymbol{k}}^{(1)}$. Once the contribution $f_{\boldsymbol{k}}^{(2)}$ has been found, it is then traced with the velocity operator, which in the crystal momentum representation is $\mathbf{v} = (1/\hbar)(\nabla_{\mathbf{k}}\varepsilon_{\boldsymbol{k}} - i[\boldsymbol{\mathcal{R}}, \mathcal{H}_{\mathrm{eff},\boldsymbol{k}}])$. The final expression for the optical current thus obtained is $\mathbf{j}_{s's}^{c} = \frac{-e}{\hbar}\sum_{ss'}\int\frac{d\mathbf{k}}{4\pi^2}\{\nabla_{\mathbf{k}}\varepsilon_{\boldsymbol{k}}^{s}\delta_{ss'} + i\boldsymbol{\mathcal{R}}_{\mathbf{k}}^{s's}[\varepsilon_{\boldsymbol{k}}^{s'} - \varepsilon_{\boldsymbol{k}}^{s}]f_{\mathbf{k},s's}^{(2)}$, where the first and second terms represent the intra- and interband contributions, respectively. Since $f_{\mathbf{k},ss'}^{(2)} \propto |\mathbf{E}|^2$ in second order, the optical current $j_{s's}^{c} \propto |\mathbf{E}|^2$. The QPE current is obtained by considering the time-independent terms in the total current. Eventually, the contribution of the off-diagonal current along the x direction is given by

$$\begin{aligned}
\mathbf{j}_{x,od}^{c} = &-\frac{e}{\hbar}\int\frac{d\mathbf{k}}{4\pi^2}(eE_x)^2\left\{\frac{\left(\mathcal{R}_{k_x}^{*,+-}\Gamma_{k_x}^{+-}\mathcal{P}_{x}^{+-} + \mathcal{R}_{k_x}^{*,+-}\partial_{k_x}\Gamma_{k_x}^{+-}(f_0(\varepsilon_{\mathbf{k}}^{+}) - f_0(\varepsilon_{\mathbf{k}}^{-}))\right)(\varepsilon_{\mathbf{k}}^{+} - \varepsilon_{\mathbf{k}}^{-})}{\left(\varepsilon_{\mathbf{k}}^{+} - \varepsilon_{\mathbf{k}}^{-} - i\frac{\hbar}{\tau}\right)^2 - (\hbar\omega)^2}\right\} \\
&+\frac{e}{\hbar}\int\frac{d\mathbf{k}}{4\pi^2}(eE_x)^2\left\{\frac{\mathcal{R}_{k_x}^{*,+-}\Gamma_{k_x}^{+-}\mathcal{M}_{x}^{+-}\left(\left(\varepsilon_{\mathbf{k}}^{+} - \varepsilon_{\mathbf{k}}^{-} - i\frac{\hbar}{\tau}\right)^2 + (\hbar\omega)^2\right)(\varepsilon_{\mathbf{k}}^{+} - \varepsilon_{\mathbf{k}}^{-})}{\left(\left(\varepsilon_{\mathbf{k}}^{+} - \varepsilon_{\mathbf{k}}^{-} - i\frac{\hbar}{\tau}\right)^2 - (\hbar\omega)^2\right)^2\left(\varepsilon_{\mathbf{k}}^{+} - \varepsilon_{\mathbf{k}}^{-} - i\frac{\hbar}{\tau}\right)}\right\} \\
&-\frac{e}{\hbar}\int\frac{d\mathbf{k}}{4\pi^2}(eE_x)^2\left\{\frac{\mathcal{P}_{x}^{+-}\mathcal{R}_{k_x}^{*,+-}\Gamma_{k_x}^{+-}\left(\frac{\hbar}{\tau}\right)(\varepsilon_{\mathbf{k}}^{+} - \varepsilon_{\mathbf{k}}^{-})}{\left(\left(\frac{\hbar}{\tau}\right)^2 + (\hbar\omega)^2\right)\left(\frac{\hbar}{\tau} + i(\varepsilon_{\mathbf{k}}^{+} - \varepsilon_{\mathbf{k}}^{-})\right)}\right\},
\end{aligned} \tag{14}$$

where we define

$$\begin{aligned}
\mathcal{P}_{x}^{ss'} &= \left[\partial_{k_x} f_0(\varepsilon_{\mathbf{k}}^{s}) - \partial_{k_x} f_0(\varepsilon_{\mathbf{k}}^{s'})\right], \\
\mathcal{M}_{x}^{ss'} &= \left[\partial_{k_x}\varepsilon_{\mathbf{k}}^{s} - \partial_{k_x}\varepsilon_{\mathbf{k}}^{s'} + \frac{i\hbar}{\tau^2}\partial_{k_x}\tau(\mathbf{k})\right] \\
&\quad\times\left[f_0(\varepsilon_{\mathbf{k}}^{s}) - f_0(\varepsilon_{\mathbf{k}}^{s'})\right],
\end{aligned} \tag{15}$$

and $\mathcal{R}_{k_x}^{+-} = \langle u_{\boldsymbol{k}}^{+}|i\partial_{k_x}|u_{\boldsymbol{k}}^{-}\rangle$. Notice that we obtain a similar expression for the the contribution of the off-diagonal current along the y direction. Although the Berry connection is gauge dependent, the optical current involves only its off-diagonal matrix elements, which can be expressed in terms of interband velocity matrix elements and are gauge covariant. Hence the final result for the current is gauge invariant, as expected. We stress that the optical current is not captured fully by Fermi's golden rule since the latter contains only band off-diagonal elements of the position operator.

III. RESULTS AND DISCUSSION

We now discuss our results for the QPE, its parameter dependence, and its physical interpretation. To begin, the QPE current along the x and y directions is shown in Fig. 1 as a function of the incident light frequency using a conservative estimate of $\tau = 39$ ps. This ensures that even for a Fermi energy of 1 meV, the condition $\varepsilon_F\tau/\hbar \gg 1$ is satisfied, so the subbands are well-defined and the kinetic equation is applicable. The longitudinal current ($\hat{x}$ direction) is accompanied by a smaller nonlinear anomalous Hall current ($\hat{y}$ direction). Hole mobilities can be orders of magnitude larger than the conservative estimate used in Fig. 1 [53,75–79], leading to much larger peaks. The effect can be easily measured in widely available semiconductors such as GaAs.

The physical explanation for the QPE is as follows. First, owing to the linear-$\boldsymbol{k}$ dependence of $\xi_{\mathbf{k}}$, the quantity $\Gamma_{k}^{+-} \neq \Gamma_{-k}^{+-}$, so the driving term is no longer symmetric in $\mathbf{k}$, and

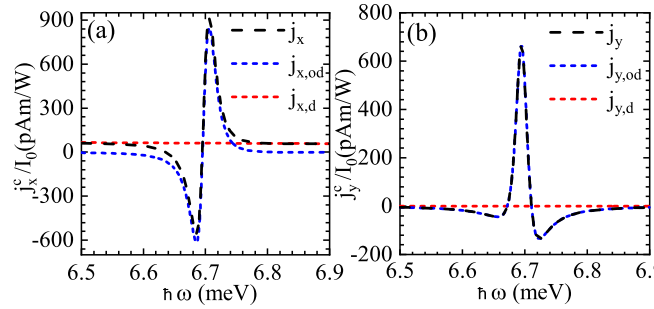

FIG. 1. The optical current j^c along (a) x and (b) y. The contributions j_d and j_{od} come from the diagonal and off-diagonal parts of the density matrix, respectively. The QPE peaks occur at $\hbar\omega = \varepsilon_{k_F}^{+} - \varepsilon_{k_F}^{-}$ and $\hbar\omega = \varepsilon_{k_F}^{+} - \varepsilon_{k_F}^{-} - \delta\omega$, where $\delta\omega = \sqrt{3/4}(\frac{\hbar}{\tau_2})^2/(\varepsilon_{k_F}^{+} - \varepsilon_{k_F}^{-})$. The peak of the nonlinear anomalous Hall current occurs at the optical transition $\hbar\omega = \varepsilon_{k_F}^{+} - \varepsilon_{k_F}^{-}$. Here $F_z = 1$ MV/m, $\tau = 39$ ps, $U_0 = 2.5$ eV m^{-1}, $n_i = 2.3\times10^{11}$ cm^{-2}, and other parameters are given in Table I in SM Sec. III. The Fermi energy $\varepsilon_F = 20.9$ meV and $k_F = 0.1$ nm^{-1} for the LH band. The HH and LH band extrema are 10.4 and 17.1 meV, respectively.

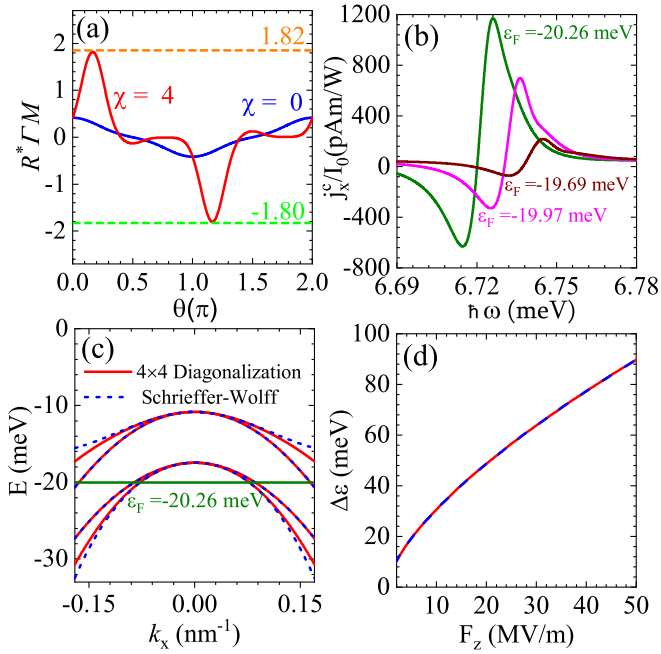

FIG. 2. (a) Anisotropy of the integrand term $\mathcal{R}^{*,+-}_{k_x}\Gamma^{+-}_{k_x}\mathcal{M}^{+-}_{x}$ as a function of θ for finite χ. Note that $\Lambda^{x,ss'}_{\boldsymbol{k}} \neq \Lambda^{x,ss'}_{-\boldsymbol{k}}$. (b) The QPE current for the different values of the Fermi energy. The scattering potential strength $U_0 = 2.5$ eV m^{-1}, the impurity density $n_i = 2.3 \times 10^{11}$ cm^{-2} and other parameters as in Fig. 1. (c) The HH and LH band structures in two different approaches. The QPE requires the Fermi energy to intersect the LH subband. (d) The variation of the LH-HH energy splitting with the top gate field F_z.

this results in an imbalance in the excited population between $\mathbf{k}$ and $-\mathbf{k}$. Since $\mathbf{E}$ lies along x ([100]), the term $(v_x n^{\text{eff}}(k) - v_x n^{\text{eff}}(-k))\tau$ corresponds to the displacement of excited holes. Here v_x is the band group velocity, which is approximately symmetric, while $n^{\text{eff}}(k)$ is the excited hole density. The surface energy at $\varepsilon^{+}_{k_F}$ oscillates under the action of the time-dependent electric field along x ([100]), resulting in different hole populations along $+k_x$ and $-k_x$. This gives rise to a net current that clearly depends on χ and on the momentum relaxation time. We emphasize that the QPE vanishes if the quadrupole term χ is neglected.

The QPE resonance occurs only for hole excitation around $\varepsilon^{+}_{k_F}$. There are two optical transitions associated with two peaks given by the denominator of the QPE current terms, which have the form $(\varepsilon^{+}_{\boldsymbol{k}} - \varepsilon^{-}_{\boldsymbol{k}} - i\hbar\tau^{-1} - \hbar\omega)$ and $(\varepsilon^{+}_{\boldsymbol{k}} - \varepsilon^{-}_{\boldsymbol{k}} - i\hbar\tau^{-1})^2 - (\hbar\omega)^2$; the direct interband transition between the LH and HH bands with the k position around the intersection of the Fermi energy and the LH band, $\hbar\omega = \varepsilon^{+}_{k_F} - \varepsilon^{-}_{k_F}$, and another transition that consists of an intraband transition with relaxation time around the Fermi energy and then an interband transition between the LH and HH bands, $\hbar\omega = \varepsilon^{+}_{k_F} - \varepsilon^{-}_{k_F} - \sqrt{3/4}(\hbar\tau^{-1})^2/(\varepsilon^{+}_{k_F} - \varepsilon^{-}_{k_F})$. The second process is forbidden between the conduction and valence bands due to Pauli blocking in a semiconductor.

The main contribution to the QPE along the x direction stems from the second term in Eq. (14), in which the integrand is anisotropic in the angle θ, as shown in Fig. 2(a). It yields a finite optical current for finite χ, caused by the asymmetric velocity distributions in the bands as a result of kinetic processes. When $\chi = 0$, the velocity of particles for the HH and LH bands is the same, the displacements of the LH and HH Fermi surfaces cancel out, and the QPE vanishes. An additional contribution to the QPE arises from Fermi surface oscillations that occur upon optical excitation owing to the difference between the HH and LH effective masses: this likewise produces a resonant current peak upon inter-subband absorption in GaAs. Our analytical calculations show that the injection current contribution [12] is proportional to $\mathcal{R}^{*,+-}_{k_x}\Gamma^{+-}_{k_x}\mathcal{M}^{+-}_{x}(\mathbf{k})(f^{(0)}(\varepsilon^{+}_{k_F}) - f^{(0)}(\varepsilon^{-}_{k_F}))$, which is the dominant contribution to the QPE. In addition, the higher-order pole current contribution is well-defined by $\frac{\partial\tau}{\partial k_x}\mathcal{R}^{*,+-}_{k_x}\Gamma^{+-}_{k_x}(\varepsilon^{+}_{k_F} - \varepsilon^{-}_{k_F})(f^{(0)}(\varepsilon^{+}_{k_F}) - f^{(0)}(\varepsilon^{-}_{k_F}))$. We obtain that the injection contribution as well as the higher-order pole current are particular contributions to obtain the nonlinear optical response along the x and y directions. However, the anomalous current and double resonant current are proportional to $\mathcal{P}^{+-}(\mathbf{k})$ and are therefore negligible.

The direction of the longitudinal QPE is set by the interplay of T_d symmetry with the applied electric field. T_d symmetry implies that, for example, x is not equivalent to $-x$, while the orientation of the external electric fields determine the direction of the current as x or $-x$. A quadrupolar Hall current is also present, driven by the same mechanism as the longitudinal current. However, there is a slight asymmetry in J_y as compared to J_{-y} due to the anisotropy of the integrand as explained in Ref. [74]. The ratio of the quadrupolar longitudinal and Hall currents is determined by crystal symmetry and depends on the electric field direction: for $\mathbf{E} \parallel [110]$ they are the same.

Next, we study the effects of the Fermi energy and relaxation time on the optical transitions. Increasing the magnitude of the Fermi energy ε_F increases the Fermi surface area, resulting in a larger peak for the photovoltaic effect current, as shown in Fig. 2(b). The main peak occurs at the optical band edge. In addition, with increasing Fermi energy, there is a redshift in the QPE. We concentrate on the band structure shown in Fig. 2(c) at a given Fermi energy. There is no optical response if the Fermi energy does not intersect the LH band. As $\hbar\omega$ approaches $\varepsilon^{+}_{k_F} - \varepsilon^{-}_{k_F}$, a hole can be excited from the LH to the HH subband. Furthermore, the optical transition point resonance varies depending on the gap between the LH and HH subbands. This gap can be tuned over the entire THz range (1–100 meV) by changing the gate electric field F_z, Fig. 2(d) [80].

We show the maximum peak value of the QPE along x as a function of the Fermi energy averaged over θ in Fig. 3(a) for different impurity strengths U_0. The peak decreases with increasing U_0. Since $\mathcal{M}^{+-}(\mathbf{k})$ is directly related to the band velocity difference between HH and LH, the current increases with increasing Fermi energy, then shows a maximum at a certain value of the Fermi energy depending on the curvatures of the band structure, following which it decreases. In Fig. 3(b), we show the peak of the QPE current as a function of the mean relaxation time averaged over the angle θ $\langle\tau(k_F)\rangle = (1/2\pi)\int_0^{2\pi}\tau(k_F,\theta)d\theta$ for a given Fermi energy ε_F. To get the height of the peak, we identify the dominant term in the

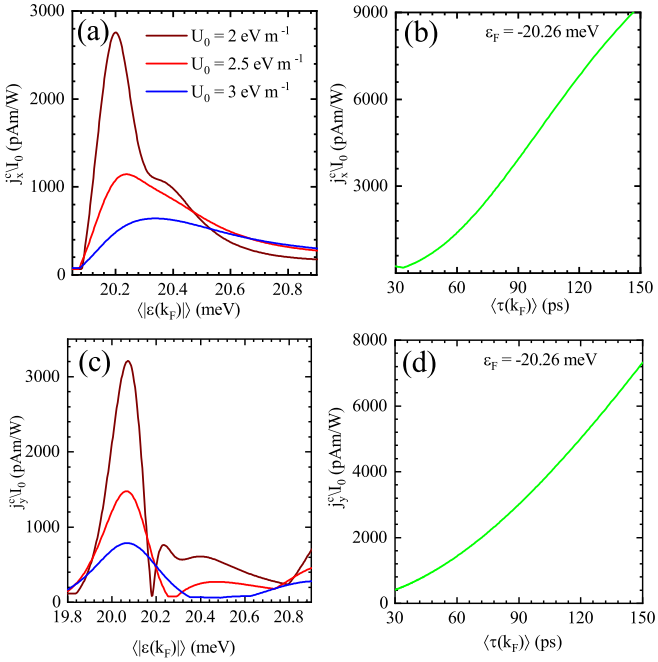

FIG. 3. The peak value of the photovoltaic response along the $\hat{\boldsymbol{x}}$ direction as a function of (a) the Fermi energy averaged over θ for different values of U_0 and (b) the scattering time $\langle\tau(k_F)\rangle$ averaged over θ at $\varepsilon_F = 20.26$ meV. (c) and (d) are the same as (a) and (b), respectively, for the peak value of the photovoltaic response along the y direction. We set $n_i = 2.3 \times 10^{11}$ cm^{-2}, $F_z = 1$ MV/m, and other parameters are given in Table III in SM Sec. III.

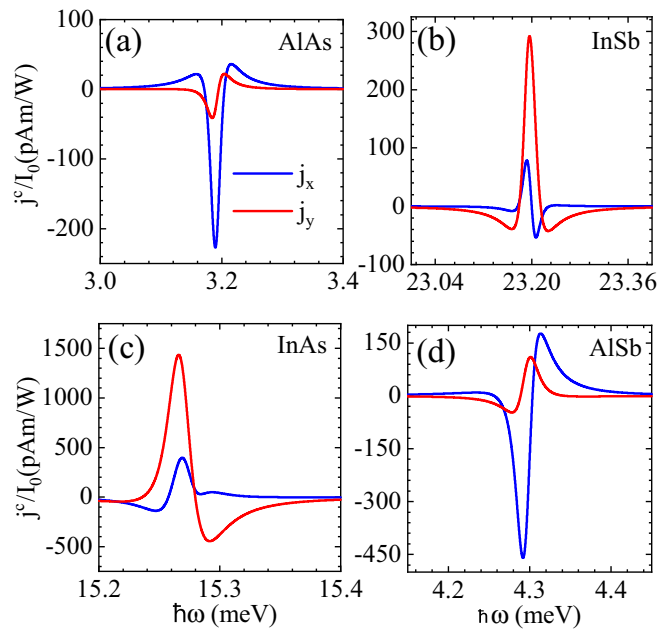

FIG. 4. The optical current j^c along the x and y directions for various zinc-blende QW semiconductors. For all cases, we set $F_z = 1$ MV/m, $\langle\tau\rangle = 39$ ps, $k_F = 0.1$ nm^{-1} and other parameters are given in Table II in SM Sec. I.

QPE as

$$\mathbf{j}^c_{x,od} \propto \frac{\omega\tau^2}{\hbar}\left[\frac{\partial f(\varepsilon^+_{\boldsymbol{k}})}{\partial k_x} - \frac{\partial f(\varepsilon^-_{\boldsymbol{k}})}{\partial k_x} + \frac{i\hbar}{\tau^2}\frac{\partial\tau(\mathbf{k})}{\partial k_x}\right]_{k=k_F,\theta=\pi}, \tag{16}$$

where only the real part is taken. There is excellent agreement between our numerics and Eq. (16). Similar explanations for the height of the peak also apply to the current along the y direction, as shown in Figs. 3(c) and 3(d).

The calculated QPE peak, using conservative figures for the hole mobility, is already considerably stronger than the photovoltaic shift current expected in topological insulators of $J/I_0 \sim 0.13$ nAm/W [6], while the experiment by Okada *et al.* [81] obtained $J/I_0 \sim 10^{-3}$ nAm/W for topological insulators. In the best-quality GaAs hole samples recently reported in Ref. [53], the measured hole mobility was 3.6×10^6 cm^{-2}/Vs, yielding $\tau = m^*\mu/e \sim 0.2$ ns. This value of τ yields a QPE peak of 20 nAm/W which is two orders of magnitude larger than in topological materials. For the sake of completeness, we have also compared GaAs with the most common zinc-blende semiconductors. The III-V zinc-blende QW semiconductors including AlAs, InSb, InAs, and AlSb exhibit a strong QPE current along x and y directions due to optical transitions between the lowest LH and HH subbands as shown in Fig. 4. GaAs semiconductor exhibit the highest QPE peaks along the x and y directions when τ, U_0, and χ are set to the identical values, with the exception of InAs, whose peak along the y direction is bigger than that in GaAs for given k_F. The band group velocity in InAs is higher than that in GaAs, and as a result, the $\mathcal{R}^{*,+-}_{k_y}\Gamma^{+-}_{k_x}\mathcal{M}^{+-}_x$ along the y direction is bigger.

It is important to consider that QW systems without a center of inversion (crystals with point group T_d) in their underlying crystal structures inherently exhibit the Dresselhaus spin-orbit interaction. Therefore, we extend our study to explore the QPE when both Rashba and Dresselhaus interactions are present. The Dresselhaus spin-orbit interaction, for $J = \frac{3}{2}$ holes is given by [59,82]

$$\begin{aligned}\mathcal{H}_D =& C_{D_1}k_x\{J_x, J_y^2 - J_z^2\} + B_{D_1}k_x(k_y^2 - k_z^2)J_x \\ &+ B_{D_2}k_x(k_y^2 - k_z^2)J_x^3 + B_{D_3}k_x(k_y^2 + k_z^2)\{J_x, J_y^2 - J_z^2\} \\ &+ B_{D_4}k_x^3\{J_x, J_y^2 - J_z^2\} + cp,\end{aligned} \tag{17}$$

where cp denotes cyclic permutation of the Cartesian coordinate elements in each term and C_{D_1} is the bulk linear k coefficient, B_{D_i} with $i = 1, 2, 3$, and 4 are the bulk cubic-k Dresselhaus coefficients. The terms with prefactors C_{D_1} and B_{D_1} dominate for common experimental density, while the remaining terms are around two orders of magnitude less and frequently ignored. Now, we add $\mathcal{H}_D$ to the band Hamiltonian and project $\mathcal{H} + \mathcal{H}_D$ onto the HH and LH bands using the Schrieffer-Wolff transformation. We then obtain an effective 2×2 Hamiltonian in the HH and LH subspace given by Eq. (155) in SM Sec. VII. Although the band energy did not change considerably, the Berry connection significantly changed by including $\mathcal{H}_D$ to the Hamiltonian. This leads to a quantitative change in $\mathcal{R}^{*,+-}_{\mathbf{k}}\Gamma^{+-}_{\mathbf{k}}$ as shown in Fig. 12 in SM Sec. VII. Moreover, our numerical results show that when the coefficient $B_{D_i} = 0$ with $i = 2$, 3, and 4, the term $\mathcal{R}^{+-}_{\mathbf{k}}$ will be reduced by 20%. The nonlinear optical current along the x and

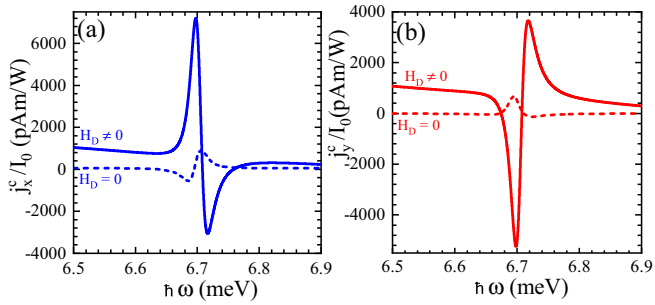

FIG. 5. The optical current j along the x and y directions induced by a time-dependent in-plane electric field $\boldsymbol{E} = E_x \cos(\omega t)\hat{x}$ in the presence (i.e., $\mathcal{H}_D \neq 0$) and absence (i.e., $\mathcal{H}_D = 0$) of the Dresselhaus spin-orbit interaction. Here, $F_z = 1$ MV/m, $\tau = 39$ ps, $U_0 = 2.5$ eV. m^{-1}, $n_i = 2.3 \times 10^{11}$ cm^{-2}.

y directions is shown in Fig. 5 as a function of the incident light frequency using both the total Rashba and Dresselhaus spin-orbit interactions provided by $\mathcal{H} + \mathcal{H}_D$ and that when only $\mathcal{H}$ is considered. As can be observed, the Dresselhaus spin-orbit interaction greatly increases the QPE peak. It has become clear that quantum nonlinear effects are sensitive to changes in the Hamiltonian parameters [83] or external perturbations of the system [11]. Here, we conclude that the Berry connection is enhanced by a factor of 2.5 due to the Dresselhaus spin-orbit interaction, and thus the photovoltaic peak rises.

We have focused on zero temperature, where phonon scattering is negligible. At higher temperatures phonons limit τ [84] and give rise to intraband transitions [85,86], making photovoltaic effects temperature dependent. Experimentally, the photovoltaic current for GaAs depends nonmonotonically on temperature [85], while theory showed that phonons cause the bulk photovoltaic current in GeTe to decrease with increasing temperature [87].

IV. CONCLUSION

We have identified a strong resonance in the second-order optical response of doped spin-$\frac{3}{2}$ hole QWs in zinc-blende materials due to a unique quadrupolar interaction with electric fields. The size and width of the resonance peak are determined by the momentum relaxation time, making the effect very strong in high-mobility systems. The existence of this peak in the photovoltaic response is intimately tied to these tetrahedral symmetry terms, which go beyond the Luttinger Hamiltonian and lead to a quadrupole interaction with electric fields. In addition, we have demonstrated that the material characteristics and the relaxation time both affect the quadrupolar photovoltaic amplitude and it greatly increases by adding the Dresselhaus spin-orbit interaction. Since the HH-LH splitting can be tuned by a top gate over the entire terahertz range, the effect can serve as the basis for a terahertz photodetector. Running this process in reverse could result in a source of terahertz radiation. Our method can also be generalized to study spin and orbital magnetic effects in the nonlinear optical response of hole QWs [88–90].

ACKNOWLEDGMENTS

We thank Roger Lewis for an enlightening and pedagogical discussion. D.C. is supported by the Australian Research Council Centre of Excellence in Future Low-Energy Electronics Technologies (Project No. CE170100039). W.A.C. acknowledges funding from the Natural Sciences and Engineering Research Council of Canada and from the Fonds de Recherche—Nature et Technologies (Quebec).

[1] R. W. Boyd, *Nonlinear Optics* (Elsevier Science and Technology, Academic Press, London, 2020)
[2] M. G. Papadopoulos, A. J. Sadlej, and J. Leszczynski, *Nonlinear Optical Properties of Matter* (Springer, Dordrecht, The Netherlands, 2006).
[3] M. Green, *Third Generation Photovoltaics* (Springer, Berlin, 2006).
[4] T. Morimoto and N. Nagaosa, Sci. Adv. **2**, e1501524 (2016).
[5] H. Watanabe and Y. Yanase, Phys. Rev. X **11**, 011001 (2021).
[6] K. W. Kim, T. Morimoto, and N. Nagaosa, Phys. Rev. B **95**, 035134 (2017).
[7] T. Morimoto and N. Nagaosa, Phys. Rev. B **94**, 035117 (2016).
[8] E. Dobardžić, M. Dimitrijević, and M. V. Milovanović, Phys. Rev. B **91**, 125424 (2015).
[9] D. Culcer, A. C. Keser, Y. Li, and G. Tkachov, 2D Mater. **7**, 022007 (2020).
[10] L. E. Golub, E. L. Ivchenko, and B. Spivak, Phys. Rev. B **102**, 085202 (2020).
[11] R. Asgari and D. Culcer, Phys. Rev. B **105**, 195418 (2022).
[12] P. Bhalla, K. Das, D. Culcer, and A. Agarwal, Phys. Rev. Lett. **129**, 227401 (2022).
[13] Z. Z. Du, C. M. Wang, H.-Z. Lu, and X. C. Xie, Nat. Commun. **10**, 3047 (2019).
[14] S. Nandy and I. Sodemann, Phys. Rev. B **100**, 195117 (2019).
[15] I. Sodemann and L. Fu, Phys. Rev. Lett. **115**, 216806 (2015).
[16] Y. Tokura and N. Nagaosa, Nat. Commun. **9**, 3740 (2018).
[17] Y. Gao and D. Xiao, Phys. Rev. Lett. **122**, 227402 (2019).
[18] L. D. Tzuang, K. Fang, P. Nussenzveig, S. Fan, and M. Lipson, Nat. Photonics **8**, 701 (2014).
[19] L. Shao, W. Mao, S. Maity, N. Sinclair, Y. Hu, L. Yang, and M. Lončar, Nat. Electron. **3**, 267 (2020).
[20] V. Belinicher and B. I. Sturman, Soviet Physics Uspekhi **23**, 199 (1980).
[21] V. Belinicher, Phys. Lett. A **66**, 213 (1978).
[22] E. L. Ivchenko, Y. B. Lyanda-Geller, G. E. Pikus, and R. Y. Rasulov, Fizika i Tekhnika Poluprovodnikov **18**, 93 (1984).
[23] J. B. Khurgin, J. Opt. Soc. Am. B **11**, 2492 (1994).
[24] R. von Baltz and W. Kraut, Phys. Rev. B **23**, 5590 (1981).
[25] V. Fridkin, Crystallogr. Rep. **46**, 654 (2001).
[26] T. Rangel, B. M. Fregoso, B. S. Mendoza, T. Morimoto, J. E. Moore, and J. B. Neaton, Phys. Rev. Lett. **119**, 067402 (2017).
[27] T. H. Maiman, Nature (London) **187**, 493 (1960).

[28] P. A. Franken, A. E. Hill, C. W. Peters, and G. Weinreich, Phys. Rev. Lett. **7**, 118 (1961).
[29] B. M. Fregoso, Phys. Rev. B **100**, 064301 (2019).
[30] G. B. Osterhoudt, L. K. Diebel, M. J. Gray, X. Yang, J. Stanco, X. Huang, B. Shen, N. Ni, P. J. Moll, Y. Ran, and K. S. Burch, Nat. Mater. **18**, 471 (2019).
[31] M. Nakamura, S. Horiuchi, F. Kagawa, N. Ogawa, T. Kurumaji, Y. Tokura, and M. Kawasaki, Nat. Commun. **8**, 1 (2017).
[32] Y. Zhang, T. Ideue, M. Onga, F. Qin, R. Suzuki, A. Zak, R. Tenne, J. Smet, and Y. Iwasa, Nature (London) **570**, 349 (2019).
[33] B. R. Carvalho, Y. Wang, K. Fujisawa, T. Zhang, E. Kahn, I. Bilgin, P. M. Ajayan, A. M. De Paula, M. A. Pimenta, S. Kar, H. C. Vincent, T. Mauricio, and L. M. Malard, Nano Lett. **20**, 284 (2020).
[34] J. E. Sipe and A. I. Shkrebtii, Phys. Rev. B **61**, 5337 (2000).
[35] S. Y. Yang, J. Seidel, S. Byrnes, P. Shafer, C.-H. Yang, M. Rossell, P. Yu, Y.-H. Chu, J. Scott, J. Ager, L. W. Martin, and R. Ramesh, Nat. Nanotechnol. **5**, 143 (2010).
[36] L. Wang, L. Huang, W. C. Tan, X. Feng, L. Chen, X. Huang, and K.-W. Ang, Small Methods **2**, 1700294 (2018).
[37] T. Oka and H. Aoki, Phys. Rev. B **79**, 081406(R) (2009).
[38] M. A. Green, Nat. Rev. Phys. **2**, 172 (2020).
[39] A. Rogalski, *Infrared Detectors* (CRC Press, London, 2000).
[40] A. Rogalski, in *Mid-infrared Optoelectronics* (Elsevier, Duxford, 2020), pp. 235–335.
[41] H. Yang, Y. Ma, Y. Liang, B. Huang, and Y. Dai, ACS Appl. Mater. Interfaces **11**, 37901 (2019).
[42] W. Lei, J. Antoszewski, and L. Faraone, Appl. Phys. Rev. **2**, 041303 (2015).
[43] A. Rogalski, Rep. Prog. Phys. **68**, 2267 (2005).
[44] M. Manfra, L. Pfeiffer, K. West, R. De Picciotto, and K. Baldwin, Appl. Phys. Lett. **86**, 162106 (2005).
[45] S. Chesi, G. F. Giuliani, L. P. Rokhinson, L. N. Pfeiffer, and K. W. West, Phys. Rev. Lett. **106**, 236601 (2011).
[46] B. Habib, M. Shayegan, and R. Winkler, Semicond. Sci. Technol. **24**, 064002 (2009).
[47] A. Srinivasan, D. S. Miserev, K. L. Hudson, O. Klochan, K. Muraki, Y. Hirayama, D. Reuter, A. D. Wieck, O. P. Sushkov, and A. R. Hamilton, Phys. Rev. Lett. **118**, 146801 (2017).
[48] R. Winkler, S. J. Papadakis, E. P. De Poortere, and M. Shayegan, Phys. Rev. Lett. **85**, 4574 (2000).
[49] F. Nichele, S. Chesi, S. Hennel, A. Wittmann, C. Gerl, W. Wegscheider, D. Loss, T. Ihn, and K. Ensslin, Phys. Rev. Lett. **113**, 046801 (2014).
[50] J. H. Cullen, P. Bhalla, E. Marcellina, A. R. Hamilton, and D. Culcer, Phys. Rev. Lett. **126**, 256601 (2021).
[51] H. Liu, E. Marcellina, A. R. Hamilton, and D. Culcer, Phys. Rev. Lett. **121**, 087701 (2018).
[52] E. Marcellina, P. Bhalla, A. R. Hamilton, and D. Culcer, Phys. Rev. B **101**, 121302(R) (2020).
[53] Y. J. Chung, C. Wang, S. K. Singh, A. Gupta, K. W. Baldwin, K. W. West, M. Shayegan, L. N. Pfeiffer, and R. Winkler, Phys. Rev. Mater. **6**, 034005 (2022).
[54] C. Gradl, R. Winkler, M. Kempf, J. Holler, D. Schuh, D. Bougeard, A. Hernández-Mínguez, K. Biermann, P. V. Santos, C. Schüller, and T. Korn, Phys. Rev. X **8**, 021068 (2018).
[55] A. Chatterjee, P. Stevenson, S. De Franceschi, A. Morello, N. P. de Leon, and F. Kuemmeth, Nat. Rev. Phys. **3**, 157 (2021).
[56] M. Veldhorst, C. Yang, J. Hwang, W. Huang, J. Dehollain, J. Muhonen, S. Simmons, A. Laucht, F. Hudson, K. M. Itoh, A. Morello, and A. S. Dzurak, Nature (London) **526**, 410 (2015).
[57] N. Hendrickx, D. Franke, A. Sammak, G. Scappucci, and M. Veldhorst, Nature (London) **577**, 487 (2020).
[58] F. N. M. Froning, M. J. Rančić, B. Hetényi, S. Bosco, M. K. Rehmann, A. Li, E. P. A. M. Bakkers, F. A. Zwanenburg, D. Loss, D. M. Zumbühl, and F. R. Braakman, Phys. Rev. Res. **3**, 013081 (2021).
[59] R. Winkler, *Spin-Orbit Coupling in Two-Dimensional Electron and Hole Systems* (Springer, Heidelberg, 2003), Vol. 41.
[60] P. Philippopoulos, S. Chesi, D. Culcer, and W. A. Coish, Phys. Rev. B **102**, 075310 (2020).
[61] E. L. Ivchenko, A. Y. Kaminski, and U. Rössler, Phys. Rev. B **54**, 5852 (1996).
[62] R. Winkler, Phys. Rev. B **70**, 125301 (2004).
[63] B. I. Sturman, V. M. Fridkin, and J. Bradley, *The Photovoltaic and Photorefractive Effects in Noncentrosymmetric Materials* (Routledge, London, 2021).
[64] E. L. Ivchenko, *Optical Spectroscopy of Semiconductor Nanostructures* (Alpha Science Int'l Ltd., Harrow, UK, 2005).
[65] S. Dhillon, M. Vitiello, E. Linfield, A. Davies, M. C. Hoffmann, J. Booske, C. Paoloni, M. Gensch, P. Weightman, G. Williams, E. Castro-Camus10, D. R. S. Cumming, F. Simoens, I. Escorcia-Carranza, J. Grant, S. Lucyszyn, M. Kuwata-Gonokami, K. Konishi, M. Koch, C. A. Schmuttenmaer *et al.*, J. Phys. D: Appl. Phys. **50**, 043001 (2017).
[66] R. Lewis, J. Phys. D **52**, 433001 (2019).
[67] J. Liu, F. Xia, D. Xiao, F. J. Garcia de Abajo, and D. Sun, Nat. Mater. **19**, 830 (2020).
[68] A. Arora, J. F. Kong, and J. C. W. Song, Phys. Rev. B **104**, L241404 (2021).
[69] W. W. Chow and S. W. Koch, *Semiconductor-Laser Fundamentals: Physics of the Gain Materials* (Springer Science & Business Media, Heidelberg 1999).
[70] B. I. Sturman, Phys. Usp. **63**, 407 (2020).
[71] D. Culcer, A. Sekine, and A. H. MacDonald, Phys. Rev. B **96**, 035106 (2017).
[72] A. Sekine, D. Culcer, and A. H. MacDonald, Phys. Rev. B **96**, 235134 (2017).
[73] P. Bhalla, A. H. MacDonald, and D. Culcer, Phys. Rev. Lett. **124**, 087402 (2020).
[74] See Supplemental Material at http://link.aps.org/supplemental/10.1103/PhysRevB.107.085405 for more details and also Refs. [6,14,59,60,91–93] therein.
[75] A. Davies, J. Frost, D. Ritchie, D. Peacock, R. Newbury, E. Linfield, M. Pepper, and G. Jones, J. Cryst. Growth **111**, 318 (1991).
[76] B. Kane, L. Pfeiffer, K. West, and C. Harnett, Appl. Phys. Lett. **63**, 2132 (1993).
[77] M. Simmons, A. Hamilton, S. Stevens, D. Ritchie, M. Pepper, and A. Kurobe, Appl. Phys. Lett. **70**, 2750 (1997).
[78] A. Dobbie, M. Myronov, R. Morris, A. Hassan, M. Prest, V. Shah, E. Parker, T. Whall, and D. Leadley, Appl. Phys. Lett. **101**, 172108 (2012).
[79] E. Sigle, D. Weißhaupt, M. Oehme, H. Funk, D. Schwarz, F. Berkmann, and J. Schulze, in *2021 44th International Convention on Information, Communication and Electronic Technology (MIPRO)* (IEEE, Opatija, Croatia, 2021), pp. 40–44.

[80] The model presented here, based on Airy functions, cannot go down to ultrasmall gate fields, hence we have truncated the lowest energy at 1 meV.
[81] K. N. Okada, N. Ogawa, R. Yoshimi, A. Tsukazaki, K. S. Takahashi, M. Kawasaki, and Y. Tokura, Phys. Rev. B **93**, 081403(R) (2016).
[82] G. Dresselhaus, Phys. Rev. **100**, 580 (1955).
[83] F. Mahmoudi and R. Asgari, Phys. Rev. B **105**, 085403 (2022).
[84] C. Rodrigues, A. Fonseca, D. Agrello, and O. Nunes, Superlattices Microstruct. **29**, 33 (2001).
[85] A. Andrianov, E. Ivchenko, G. Pikus, R. Y. Rasulov, and I. Yaroshetskil, Zh. Eksp. Teor. Fiz **81**, 2080 (1981).
[86] V. Belinicher, E. Ivchenko, and B. Sturman, Zh. Eksp. Teor. Fiz **83**, 649 (1982).
[87] S.-J. Gong, F. Zheng, and A. M. Rappe, Phys. Rev. Lett. **121**, 017402 (2018).
[88] J. Wu, H. ming Hao, Y. Liu, Y. Zhang, X. lin Zeng, S. bo Zhu, Z. chuan Niu, H. qiao Ni, and Y. hai Chen, Opt. Express **29**, 13829 (2021).
[89] V. Lechner, L. E. Golub, F. Lomakina, V. V. Bel'kov, P. Olbrich, S. Stachel, I. Caspers, M. Griesbeck, M. Kugler, M. J. Hirmer, T. Korn, C. Schüller, D. Schuh, W. Wegscheider, and S. D. Ganichev, Phys. Rev. B **83**, 155313 (2011).
[90] C. Zoth, P. Olbrich, P. Vierling, K.-M. Dantscher, V. V. Bel'kov, M. A. Semina, M. M. Glazov, L. E. Golub, D. A. Kozlov, Z. D. Kvon, N. N. Mikhailov, S. A. Dvoretsky, and S. D. Ganichev, Phys. Rev. B **90**, 205415 (2014).
[91] S. Papadakis, E. De Poortere, H. Manoharan, M. Shayegan, and R. Winkler, Science **283**, 2056 (1999).
[92] B. Habib, E. Tutuc, S. Melinte, M. Shayegan, D. Wasserman, S. Lyon, and R. Winkler, Appl. Phys. Lett. **85**, 3151 (2004).
[93] F. Stern, Phys. Rev. B **5**, 4891 (1972).